MEASUREMENT SYSTEM AND MULTI-DIMENSIONAL FLOW CHARACTERISTICS OF BUBBLY COUNTERCURRENT FLOW

- Effects of Air and Water Flow Rates -

Shirong ZHOU [1],Masanori ARITOMI [1], Junji MIZOGUCHI [2],

Yasushi TAKEDA [3] and Michitsugu MORI [4]

1 Tokyo Institute of Technology, 2-12-1 Ohokayama, Meguro-ku, Tokyo, 152 Japan
TEL +81-3-5734-3063, FAX +81-3-5734-2959

2 Shibaura Institute of Technology, 307 Tameihara, Fukasaku, Omiya, 330 Japan
TEL +81-48-687-5058, FAX +81-48-687-5116

3 Paul Scherrer Institut, Wurenlingen and Villigen, CH-5232, Villigen, Switzerland
TEL +41-56-310-3568, FAX +41-56-310-3131

4 Tokyo Electric Power Co., 1-1-3 Uchisaiwai-cho, Chiyoda-ku, Tokyo, 100 Japan
TEL +81-45-585-8932, FAX +81-45-585-8943

Contact person: Masanori ARITOMI
Professor
Research Laboratory For Nuclear Reactors,
Tokyo Institute of Technology
2-12-1 Ohokayama, Meguro-ku, Tokyo,152 Japan
TEL +81-3-5734-3063, FAX +81-3-5734-2959

ABSTRACT

The authors have developed a new measurement system which consisted of an ultrasonic velocity profile monitor and a video data processing unit in order to clarify its multi-dimensional flow characteristics in bubbly flow and to offer a data base to validate numerical codes for multi-dimensional two-phase flow. In this paper, the proposed measurement system was applied for fully developed bubbly countercurrent flows in a vertical rectangular channel. At first, both bubble and water velocity profiles and void fraction profiles in the channel were investigated statistically. Next, turbulence intensity in the channel was defined as a standard deviation of velocity fluctuation in a continuous liquid phase, and the two-phase multiplier profile of turbulence intensity in bubbly countercurrent flows was clarified. In addition, the distribution parameter and drift velocity used in the drift flux model were calculated directly from these profiles.

1. INTRODUCTION

In the study of two-phase flow, the knowledge of bubbly and liquid velocities is required for better understanding of transport phenomena in two-phase flow systems. The void fraction is the most important parameter for engineering use, e.g. for the design of nuclear reactors, steam boilers, evaporating equipment, refrigerating equipment, etc. Recently, many concepts of future light water reactor (LWRs), in which passive and simplified safety functions are actively introduced into their safety features, have been proposed such as the AP-600 design (Tower et al. 1988) and the SBWR design (Duncan 1988) in order to reduce their construction cost, to improve their reliability and maintainability and so on. However, since passive safety features are functioned by the law of nature, the driving force is much smaller than that induced by active ones. Multi-dimensional two-phase flow may, therefore, appear after their safety features are activated. Consequently, it is necessary with regard to passive safety features to be able to simulate multi-dimensional flow characteristics even for the two-phase flow which can be regarded as one dimensional flow for active ones.

The two-phase flow shows essentially multi-dimensional characteristics even in a simple

channel. The safety analysis codes such as the TRAC (Liles et al. 1979) and RELAP5 (Ransom et al. 1981) treat the flow basically as one dimensional flow and introduce multi-dimensional convection effects in a macroscopic way due to a lack of a fundamental data base for establishing the model of multi-dimensional two-phase flow dynamics. It is one of the important problems to establish an analytical method of multi-dimensional two-phase flow to verify analytically the effectiveness of passive safety features. It is also one of the most important subjects in the research of two-phase flow dynamics to clarify its multi-dimensional flow characteristics.

Recently, an ultrasonic Doppler method for velocity profile measurement has been developed for liquid flow measurements by Takeda (1995). It can measure a local velocity profile instantaneously as a component in the ultrasonic beam direction, so that a velocity field can be measured in space and time domain (Takeda 1994). The authors have developed a new measurement system composed of Ultrasonic Velocity Profile Monitor (UVP) and a Video Data Processing Unit (VDP) to measure multi-dimensional flow characteristics in bubbly flow (Aritomi et al. 1996), which can measure simultaneously the multi-dimensional flow characteristics of bubbly flow such as velocity profiles of both gas and liquid phases and a void fraction profile in a channel, an average bubble diameter and an average void fraction.

In this paper, the proposed measurement system was applied to fully developed bubbly countercurrent flows in a vertical rectangular channel in order to understand the multi-dimensional flow characteristics and to offer a data base to validate numerical codes for multi-dimensional two-phase flow. At first, both bubble and water velocity profiles and void fraction profiles in the channel were investigated statistically under various conditions of both air and water flow rates. Next, turbulence intensity in the channel was defined as a standard deviation of velocity fluctuation in a continuous liquid phase, and the two-phase multiplier profile of turbulence intensity in the channel was measured as a ratio of the standard deviation of velocity fluctuation in a bubbly countercurrent flow to that in a water single phase flow. In addition, concerning the drift flux model, the distribution parameter and the drift velocity

were calculated directly from these profiles, and were compared with the correlation proposed for bubbly countercurrent flows.

2. EXPERIMENTAL APPARATUS AND MEASUREMENT PRINCIPLE

2.1 Experimental Apparatus

Figure 1 shows a schematic diagram of an experimental apparatus. Air and water were used as working fluids. The experimental apparatus was composed of a water circulation system, an air supply system, a test section and a measurement system. The test section was a vertical rectangular channel of 10mmx100mmx500mm made of Plexiglas as shown in **Fig.2**. The measurement system consisted of the UVP, the VDP and a personal computer to record and treat data.

Water was fed into the upper tank and flowed downward in the test section. The water level in an upper tank was kept constant with an overflow nozzle which was connected to a lower feedwater tank. The flow rate was regulated by a flow control valve and measured by an orifice flowmeter which were installed at the downstream end of the test section. Adopting this flow control system, the water flow rate could be kept constant for hours. Microparticles of nylon powder were suspended in water to reflect ultrasonic pulses. Water temperature is kept constant by a subcooler.

The air supply system consisted of a compressor and a pressure regulation valve. Bubbles were injected from three needles located near the bottom of the channel. The air flow rate was measured by a float flowmeter and regulated by another flow control valve. As a result, the air flow rate could be kept constant for hours. Pressure transducers and thermocouples were installed at several points in the loop to monitor the flow condition. A personal computer acquired the readings from these sensors for an on-line control of the experimental condition.

An ultrasonic transducer was installed on the outside surface of the front wall of the channel with a contact angle θ of 45° and a gap between the transducer and the wall was

filled with a jelly to prevent a reflection of ultrasonic pulses on the wall surface as shown in **Fig.2**. After both air and water flow rates were set up at the desired values, 9,216 (1,024x9) velocity profiles along a measured line were measured under one experimental condition to treat them statistically. It takes about 30 minutes to get them. The hydrostatic head was simultaneously measured as a pressure drop between the pressure taps installed on the side wall using a differential pressure transducer to get an averaged void fraction.

An outline of video camera equipment is shown in **Fig.3**, which consists of an 8mm video camera, a light source and a translucent sheet to unify the luminance brightness. The speed, diaphragm and gain of the video camera can be manually regulated and a speed of 60 flames per second can be obtained. After videotaping, the video digital data were recorded in a personal computer through an image converter. The picture elements are 640x240 dots, the color is monotone, and the brightness resolution is 1/256. Since the measurement method of the VDP was described in our previous work (Aritomi et al. 1996), its description is omitted here.

The experimental conditions are tabulated in **Table 1.**

2.2 Measurement Principle of UVP

Since the detailed information of the proposed measurement system was reported in our previous work (Aritomi et al. 1996), its measurement principle is described briefly and to the point in this paper.

The working principle of the UVP is to use the echo of ultrasonic pulses reflected by microparticles suspended in the fluid. An ultrasonic transducer takes roles of both emitting ultrasonic pulses and receiving the echoes, that is, the backscattered ultrasound is received for a time interval between two emissions.

The position information, x, is obtained from the time lapse, τ, from the emission to the reception of the echo:

$$x = c\tau / 2 , \tag{1}$$

where c is a sound speed in the fluid. An instantaneous local velocity, $u_{UVP}(x_i)$, as a component in the ultrasonic beam direction, is derived from the instantaneous Doppler shift frequency, f_D, in the echo:

$$u_{UVP} = cf_D / 2f , \tag{2}$$

where f is the basic ultrasonic frequency (4MHz). The velocity resolution is 0.75mm/s for our proposed system. Horizontal position, y, and axial velocity, u, can be expressed by

$$y = \Delta x \cdot i \cdot \sin\theta , \tag{3}$$

and

$$u = u_{UVP} / \cos\theta , \tag{4}$$

where $\triangle x$ is a spatial resolution, which is 0.74 mm for our proposed system, i is the number of the reception of the emission echo.

A probability density function includes the velocity information of both phases. Assuming that each probability density function of both phases can be expressed by a normal distribution,

$$N[\bar{u},\ \sigma^2](u) = \frac{1}{\sqrt{2\pi\sigma^2}} \exp\left[-\frac{(u - \bar{u})^2}{2\sigma^2}\right] . \tag{5}$$

The probability density function of mixture velocity is given by

$$P_u(y,u) = \varepsilon(y)N[\bar{u}_G(y),\sigma_G^2(y)](u) + (1 - \varepsilon(y))N[\bar{u}_L(y),\sigma_L^2(y)](u) . \tag{6}$$

where $\bar{u}_G$ and $\bar{u}_L$ are average velocities of gas and liquid phases respectively, σ_G and σ_L

are standard deviations of both phases respectively and ε is the probability of bubble existence. These five variables, $\bar{u}_G$, $\bar{u}_L$, σ_G, σ_L and ε, are calculated numerically and iteratively by the least squares method. An example of the probability density function obtained from the UVP data is representatively shown in **Fig.4**.

As long as a bubble exists, the ultrasonic pulse is reflected at its surface, so that the bubble velocity can be always detected as the interfacial velocity. On the other hand, the ultrasonic wave is not reflected in water where a microparticle does not exist. As a result, water velocity is not always measured in the profile. Hence, it is necessary to revise the probability of bubble existence as follows:

$$\kappa(y) = P_s(y)\ \varepsilon(y), \tag{7}$$

where $P_s(y)$ is the probability of data existence. $\kappa(y)$ is called the probability of bubble data existence in this work.

The average void fraction was obtained by measuring the hydrostatic head or from the VDP data. Assuming that the local void fraction is proportional to the local probability of bubble data existence and that the proportional constant, k, is uniform in the channel since it is dependent on bubble size and configuration, the average void fraction is expressed by

$$<\alpha> = k\int_A \kappa\, dA / A = k<\kappa> . \tag{8}$$

The proportional constant, k, was calculated from measured average void fraction, $<\alpha>$, and measured average probability of bubble data existence, $<\kappa>$. Then, local void fraction, $\alpha(y)$, is given by

$$\alpha(y) = k\ \kappa(y) . \tag{9}$$

The UVP specification used in this work is tabulated in **Table 2**.

3. RESULTS AND DISCUSSION

3.1 Multi-dimensional Flow Characteristics

Velocity profiles of both phases in the channel were measured with the UVP. At first, the effects of air flow rates on flow characteristics in bubbly countercurrent flows was investigated for both low and high water flow rates. The experimental results are shown in **Figs.5(a)** and **(b)**. Since it is very difficult to measure the velocities near the wall with significant accuracy due to an ultrasonic beam diameter of 5mm, they are omitted in these figures. Water downward velocities become higher toward the center of the channel from the wall in the same tendency as water single phase flow. In contrast with this, bubble velocities are higher near the wall than those in the core. Relative velocity was defined by a difference between the bubble and water velocities. Relative velocity profiles were calculated from the results shown in **Figs.5(a)** and **(b)** and are shown in **Figs.6(a)** and **(b)**. It can be seen from these figure that the relative velocities are almost constant in the whole channel and are scarcely varied with changes in the water flow rate. It is clear from **Figs.5** and **6** that the flow characteristics of bubbly countercurrent flow is strongly dependent on the water velocity which is a continuous phase and that a bubble rising velocity is induced by the difference between the buoyancy and interfacial drag force. As a result, in fully developed bubbly countercurrent flow with the almost same bubble diameter in the channel, the relative velocities are almost equal in the whole channel. Since air flow rates are much lower than water ones under the present conditions, the velocity profiles of both phases are scarcely varied even if the air flow rate increases.

Next, the effects of water flow rates on flow characteristics in bubbly countercurrent flows was also investigated for both low and high air flow rates. The experimental results are shown in **Figs.7(a)** and **(b)**. It can be seen from the figure that water velocities become higher but their profiles are scarcely influenced with an increase in a water flow rate. However, bubble rising velocities become lower but their profiles are still hardly affected under the

present conditions. With an increase in water flow rate, an impact pressure at bubble generation nozzles becomes larger and bubble rising velocity decreases. Relative velocity profiles were calculated from the results shown in **Figs.7(a)** and **(b)** and are shown in **Figs.8(a)** and **(b)**. It can be seen from these figures that the relative velocities are almost constant in the whole channel and are scarcely varied with changes in the air flow rate.

3.2 Void Fraction Profiles

The hydrostatic head is obtained from the measured differential pressure and average void fraction is calculated by

$$(\Delta P / \Delta Z)_{Head} = \rho_G <\alpha> g + \rho_L (1 - <\alpha>) g \ , \qquad (10)$$

because friction loss is negligibly small due to low water flow rates. According to Eqs.(8), (9) and (10), $\alpha(y)$ can be calculated. The threshold brightness (Aritomi et al. 1996), which identifies the bubble surface, influences evaluation of the average bubble diameter and void fraction even though it does not affect the number of bubbles, the threshold brightness was calibrated. A comparison of average void fractions obtained by the hydrostatic head and by the VDP is shown in **Fig.9**. The void fractions obtained by the VDP agree well with those obtained by the hydrostatic head.

A bubble diameter is calculated from its volume by assuming that it is spherical. The relationship between average bubble diameters and average void fractions is shown in **Fig.10**. With an increase in a water flow rate, an impact pressure at bubble generation nozzles becomes larger and a bubble rising velocity decreases as shown in **Figs.7(a)** and **(b)**, so that the average bubble diameter becomes larger. In addition, as an air flow rate increases, the average bubble diameter increases because the air pressure in the bubble generation needles is enlarged.

Figures 11(a) and **(b)** show the typical measured results of a probability profile of bubble data existence. The probability of bubble data existence means that a bubble exists in an

ultrasonic pulse path when the pulse is emitted. It is clearly seen from the figure that the probability of bubble data existence increases with air and water flow rates increase. A void fraction profile in the channel can be calculated from Eqs.(8) and (9) and the measured probability profile of bubble data existence. The effects of air flow rates on the void fraction profile for both low and high water flow rates are shown in **Figs.12(a)** and **(b)**, respectively. It can be seen from these figures that void fraction profiles are almost flat in bubbly countercurrent flows except for those near the wall. Since air flow rates are much lower than water ones under the present experimental conditions, water velocity profiles are scarcely varied even with a change in air flow rates. As a result, bubble velocity is dependent on the water velocity profile as shown in **Figs.5** and **7**. The void fraction is, consequently, enlarged with an increase in air flow rates as shown in **Figs.12(a)** and **(b)**. This tendency appears more strongly for higher water flow rate. Next, the effects of water flow rates on the void fraction profile for both low and high air flow rates are shown in **Figs.13(a)** and **(b)**, respectively. As the water flow rate increases, the bubble rising velocity is decreased, so that void fraction becomes larger. This tendency appears more remarkably with an increase in the air flow rate.

3.3 Turbulence Intensity Profile

As a general rule, the turbulence intensity in a bubbly flow is larger than that in liquid single phase flow because bubbles agitate the flow. In this work, the turbulence intensity is defined as a standard deviation of water velocity fluctuation in a continuous liquid phase, σ_L given by Eq.(6). Typical results in a water single flow and a bubbly countercurrent flow are shown in **Figs.14** **(a)** and **(b)**, respectively. In a water downward flow, the turbulence intensity has the maximum value near the wall and becomes lower with going toward the center of the channel in the same manner as a single phase flow because the gradient of longitudinal velocities is higher near the wall. On the other hand, in a bubbly countercurrent flow, the turbulence intensity becomes higher with going toward the center of the channel and has the maximum value in the center of the channel. Fluctuation of bubble upflow in the core

is larger than that near the wall because the restriction of the boundary is weakened. This fact indicates that bubbles agitate the flow in a continuous liquid phase.

Since local velocities were measured not at a point but on the area because of an ultrasonic beam diameter of 5mm, the absolute value of the standard deviation in a water phase is not significant. Hence, The ratio of the standard deviation ratio in a bubbly countercurrent flow to that in a water single phase flow is selected as two-phase multiplier of turbulence intensity, $\sigma_{LTPF}/\sigma_{LSPF}$. **Figures 15(a)** and **(b)** show the effects of air flow rates on the two-phase multiplier of turbulence intensity for both low and high water flow rates, respectively. The two-phase multiplier of turbulence intensity becomes larger with going toward the center of the channel. It can be seen from these figures that $\sigma_{LTPF}/\sigma_{LSPF}$ are enhanced with increases in air flow rates. This tendency becomes more notable with an increase in the water flow rate.

Next, the effects of water flow rates on the profile of $\sigma_{LTPF}/\sigma_{LSPF}$ for both low and high air flow rates are illustrated in **Figs.16(a)** and **(b)**, respectively. As the water flow rate increases, the profiles of $\sigma_{LTPF}/\sigma_{LSPF}$ are scarcely varied at a low air flow rate but becomes larger at a high one.

Typical measured results of velocity profile of both phases, $u_G(y)$ and $u_L(y)$, void fraction profile, $\alpha(y)$, and two-phase multiplier profile of turbulence intensity, $\sigma_{LTPF}/\sigma_{LSPF}$ are tabulated in **Table 3** as a data base to model multi-dimensional two-phase flow and validate its numerical codes. j_L, j_G, D_b mean specific velocities of water and air and the average bubble diameter, respectively, y is the horizontal position and H is the width of the channel, 10mm.

3.4 Distribution Parameter and Drift Velocity

The drift flux model proposed by Zuber and Findlay (1965) is widely applied to two-phase flow analysis codes. The following notations are introduced:

$$\langle F \rangle = \frac{\int_A F dA}{A} \tag{11}$$

and

$$\langle F \rangle = \frac{\langle \alpha F \rangle}{\langle \alpha \rangle} \tag{12}$$

where F is a variable and A is a flow channel cross section. In the drift flux model, local drift velocity, v_{gj}, and the distribution parameter, C_0, are defined as follows:

$$v_{gj} = u_G - j \ , \tag{13}$$

and

$$C_O = \langle \alpha j \rangle / \langle \alpha \rangle \langle j \rangle \ , \tag{14}$$

where j is volumetric flux and defined by

$$j = j_G + j_L = \alpha u_G + (1 - \alpha) u_L \ . \tag{15}$$

Since it was difficult to measure velocity profiles of both phases and void fraction profiles directly, in many previous works, average void fractions were measured under various conditions of $\langle j_G \rangle$ and $\langle j_L \rangle$, and C_0 and V_{gj} were determined by

$$\frac{\langle j_G \rangle}{\langle \alpha \rangle} = C_0 \langle j \rangle + \langle v_{gj} \rangle = C_0 \langle j \rangle + V_{gj} \ . \tag{16}$$

In this work, velocity profiles of both phases and void fraction profiles can be measured. Local drift velocity is given by

$$v_{gj}(y) = [1-\alpha(y)][u_G(y) - u_L(y)] \ . \qquad (17)$$

Substituting experimental results of $u_G(y)$, $u_L(y)$ and $\alpha(y)$ into Eqs.(14), (15) and (17), the distribution parameters and the drift velocity were calculated and the results are shown in **Figs.17** and **18**, respectively. It can be seen from **Figs.12** and **13** that the void fraction profiles are nearly flat except for those near the wall. Consequently, the distribution parameter is almost 1.0. Substituting properties of air and water into the correlation proposed by Zuber and Findlay (1965), $V_{gj} = 0.231m/s$. The results shown in **Fig.18** are identical to this value.

4. CONCLUDING REMARKS

The measurement system composed of the UVP and the VDP was applied to measure flow characteristics of bubbly countercurrent flows. The following insights are clarified:

(1) Water downward velocities become higher with leaving the wall but bubble rising velocities decreases because of higher water velocities. The relative velocities between both phases are scarcely varied in the channel.

(2) Void fractions in the channel are almost constant except for those near the wall.

(3) For the bubbly countercurrent flow, the turbulence intensity is greater than that in water single phase flow and increases with going toward the center from the wall.

(4) The two-phase multiplier of turbulence intensity increases with increases in air and/or water flow rates. Moreover, the effects of air flow rates on the two-phase multiplier of turbulence intensity is greater than that of water flow rates.

(5) Concerning the drift flux model, the distribution parameter is 1.0 for bubbly countercurrent flow and the drift velocity is the same value as proposed for bubbly upflows.

This work was performed at the Tokyo Institute of Technology in collaboration with the Tokyo Electric Power Company and the Paul Scherrer Institut.

REFERENCE

Aritomi, M., Zhou, S., Nakajima, M., Takeda, Y., Mori, M., and Yoshioka, Y. (1996),

Measurement system of bubbly flow using ultrasonic velocity profile monitor and video data processing unit. J. Nucl.Sci Technol., **33** 915–923.

Duncan, J.D. (1988), SBWR: A simplified boiling water reactor. Nucl. Engrg. Des., **109**, 73–77.

Liles, D.R. et al. (1979), TRAC–P1A: An advanced best–estimate computer programs for PWR LOCA analysis. NUREG/CR–0665.

Ransom, V.H. et al. (1981), RELAP5/MOD1 code manual. Vol. 1 System and numerics, NUREG/CR–1827.

Takeda, Y. (1994), Decomposition of the modulated waves in a rotating couette system. Science, **263**, 502–505.

Takeda, Y., (1995), Velocity profile measurement by ultrasonic doppler method. Experimental Thermal and Fluid Sci., **10**, 444–453.

Tower, S.N., Schulz, T.L. and Vijuk R.P. (1988), Passive and simplified system features for the advanced westinghouse 600 MWe PWR, Nucl. Engrg. Des., **109**, 147–154.

Zuber, N. and Findlay J.A. (1965), Average volumetric concentration in two–phase flow systems, Trans. ASME, J. Heat Transfer, **87**, 453–468.

Table 1 Experimental conditions

System pressure	Atmospheric pressure
Water specific velocity	−0.06, −0.12m/s
Air specific velocity	0.00195 - 0.00418m/s

Table 2 The specification of the Ultrasonic Velocity Profile Monitor

Basic ultrasonic frequency	4MHz
Maximum measurable depth	758mm (variable)
Minimum spatial resolution	0.74mm
Maximum measurable velocity	0.75m/s (variable)
Velocity resolution	0.75mm/s (variable)
Measurement points	128
The number of profiles	1,024

Table 3 Measured results of the UVP

j_L = −0.06(*m/s*) , j_G =0.00195(*m/s*) , D_b = 3.23(*mm*)

y/(H/2)(mm)	u_G(*m/s*)	u_L(*m/s*)	α	$\sigma_{LTPF}/\sigma_{LSPF}$
0.000	0.205	−0.053	0.008	1.837
0.105	0.176	−0.059	0.010	1.558
0.211	0.169	−0.064	0.012	1.912
0.316	0.166	−0.069	0.013	2.089
0.421	0.163	−0.073	0.013	2.391
0.526	0.156	−0.075	0.014	2.739
0.632	0.150	−0.076	0.014	3.036
0.737	0.141	−0.076	0.015	3.281
0.842	0.135	−0.078	0.015	3.358
0.947	0.132	−0.080	0.015	3.347

j_L = −0.06(*m/s*) , j_G = 0.00327(*m/s*) , D_b = 3.83(*mm*)

y/(H/2)(mm)	u_G(*m/s*)	u_L(*m/s*)	α	$\sigma_{LTPF}/\sigma_{LSPF}$
0.000	0.198	−0.061	0.012	2.751
0.105	0.182	−0.066	0.015	2.325
0.211	0.170	−0.071	0.017	2.571
0.316	0.167	−0.075	0.018	2.999
0.421	0.165	−0.079	0.019	3.151
0.526	0.161	−0.082	0.020	3.412
0.632	0.156	−0.082	0.020	3.940
0.737	0.150	−0.083	0.021	4.340
0.842	0.147	−0.084	0.021	4.472
0.947	0.148	−0.085	0.020	4.387

j_L = −0.06(*m/s*) , j_G = 0.00418(*m/s*) , D_b = 4.34(*mm*)

y/(H/2)(mm)	u_G(*m/s*)	u_L(*m/s*)	α	$\sigma_{LTPF}/\sigma_{LSPF}$
0.000	0.183	−0.066	0.017	3.228
0.105	0.172	−0.073	0.020	2.810
0.211	0.165	−0.079	0.023	2.975
0.316	0.164	−0.082	0.025	3.313
0.421	0.164	−0.084	0.025	3.693
0.526	0.163	−0.087	0.026	4.067
0.632	0.159	−0.087	0.026	4.707
0.737	0.155	−0.089	0.026	5.011
0.842	0.153	−0.089	0.026	5.003
0.947	0.149	−0.092	0.026	4.797

Table 3 Measured results of the UVP

j_L = -0.12m/s) , j_G =0.00195(m/s) , D_b = 3.70(mm)

$y/(H/2)(mm)$	$u_G(m/s)$	$u_L(m/s)$	α	$\sigma_{LTPF}/\sigma_{LSPF}$
0.000	0.105	−0.097	0.017	1.304
0.105	0.094	−0.110	0.020	1.385
0.211	0.087	−0.121	0.021	1.483
0.316	0.083	−0.131	0.023	1.778
0.421	0.080	−0.136	0.024	2.260
0.526	0.068	−0.140	0.026	2.628
0.632	0.064	−0.143	0.027	3.019
0.737	0.071	−0.143	0.026	3.434
0.842	0.060	−0.144	0.027	3.407
0.947	0.070	−0.142	0.025	3.559

j_L = -0.12(m/s) , j_G = 0.00327(m/s) , D_b = 4.37(mm)

$y/(H/2)(mm)$	$u_G(m/s)$	$u_L(m/s)$	α	$\sigma_{LTPF}/\sigma_{LSPF}$
0.000	0.105	−0.092	0.033	1.677
0.105	0.098	−0.106	0.036	1.823
0.211	0.092	−0.120	0.039	1.921
0.316	0.092	−0.128	0.042	2.318
0.421	0.093	−0.134	0.043	3.009
0.526	0.096	−0.137	0.044	3.785
0.632	0.095	−0.139	0.044	4.334
0.737	0.093	−0.141	0.045	4.673
0.842	0.092	−0.141	0.045	4.916
0.947	0.089	−0.142	0.045	4.894

j_L = -0.12(m/s) , j_G = 0.00418(m/s) , D_b = 5.06(mm)

$y/(H/2)(mm)$	$u_G(m/s)$	$u_L(m/s)$	α	$\sigma_{LTPF}/\sigma_{LSPF}$
0.000	0.111	−0.104	0.049	2.269
0.105	0.108	−0.117	0.051	2.527
0.211	0.107	−0.127	0.055	2.760
0.316	0.106	−0.134	0.060	3.412
0.421	0.107	−0.134	0.062	4.311
0.526	0.110	−0.134	0.062	5.148
0.632	0.108	−0.134	0.064	6.032
0.737	0.108	−0.132	0.063	6.496
0.842	0.108	−0.130	0.064	6.666
0.947	0.107	−0.132	0.065	6.541

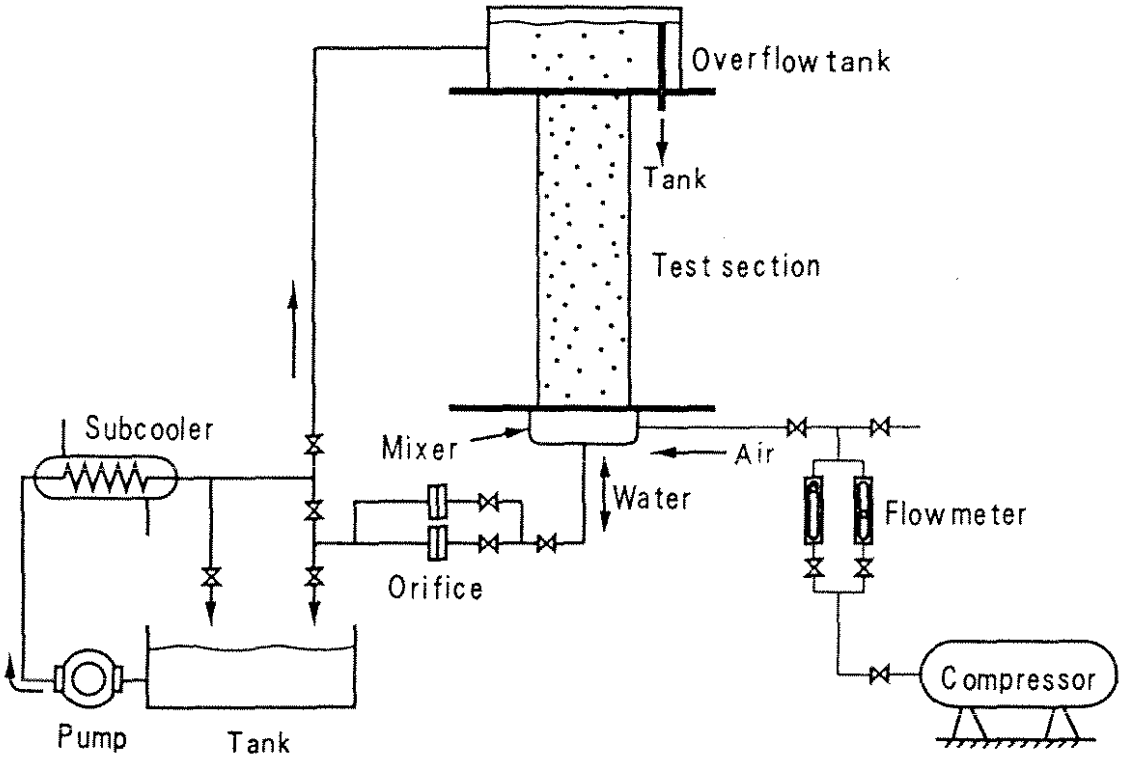

Fig.1 A schematic diagram of experimental apparatus

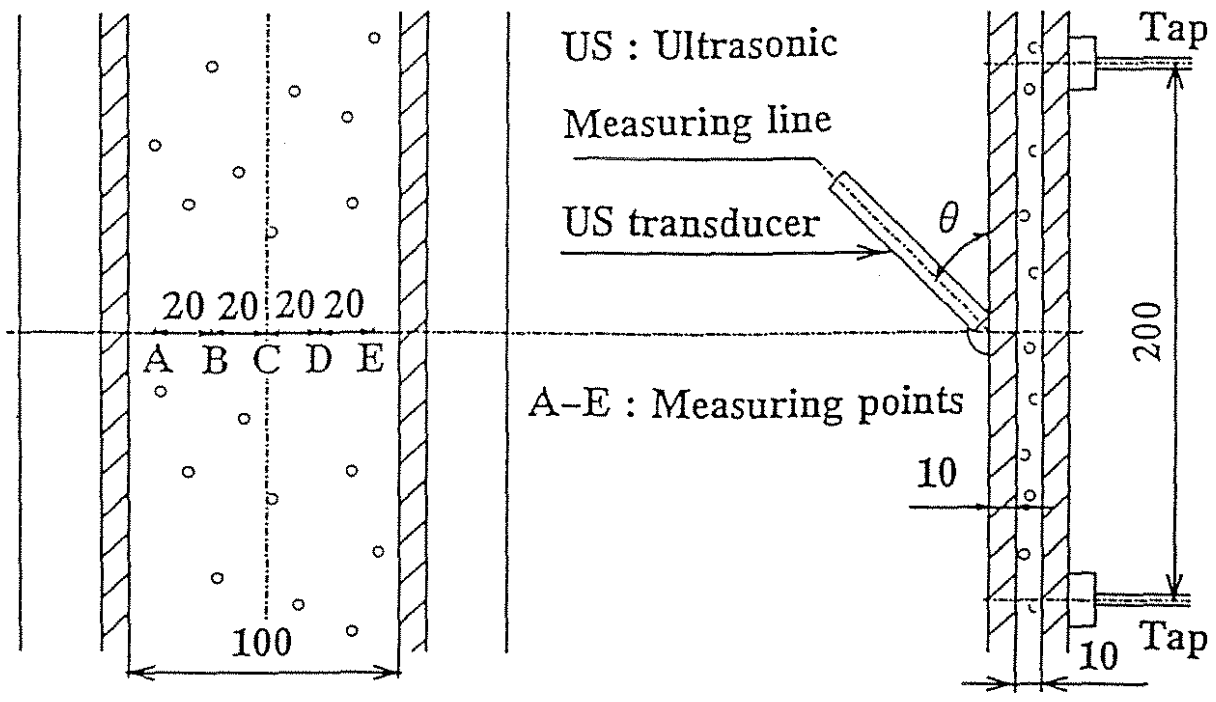

Fig.2 Test section

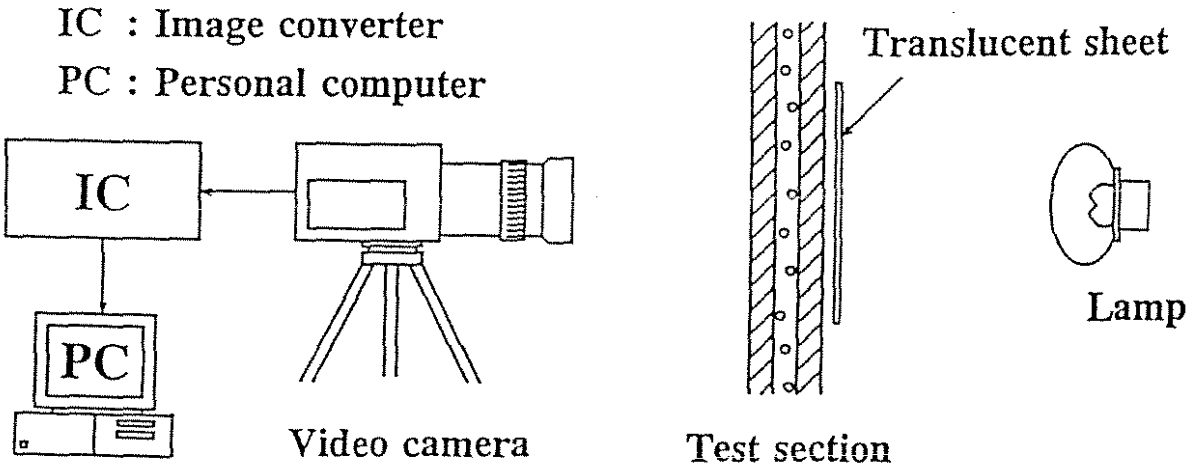

Fig.3 An outline of video camera equipment

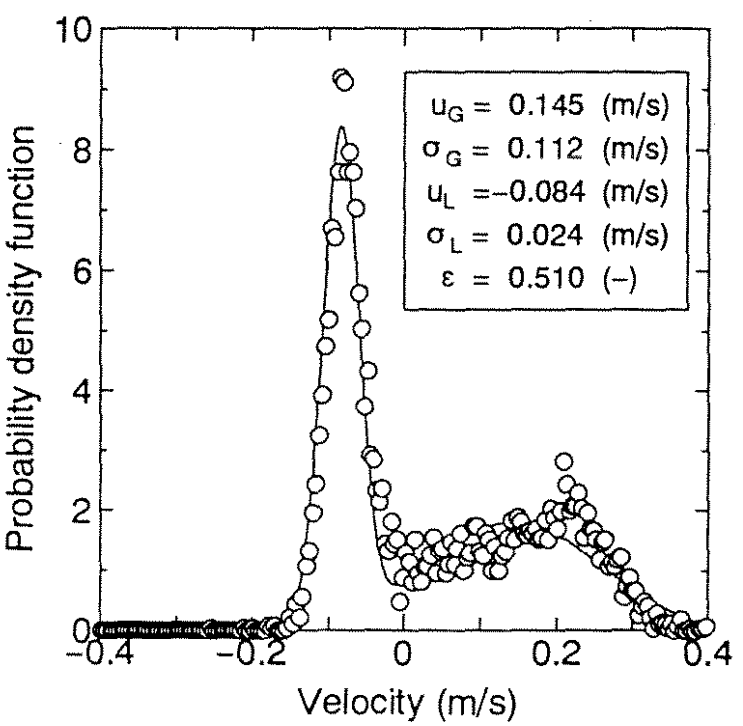

Fig. 4 A typical probability density function

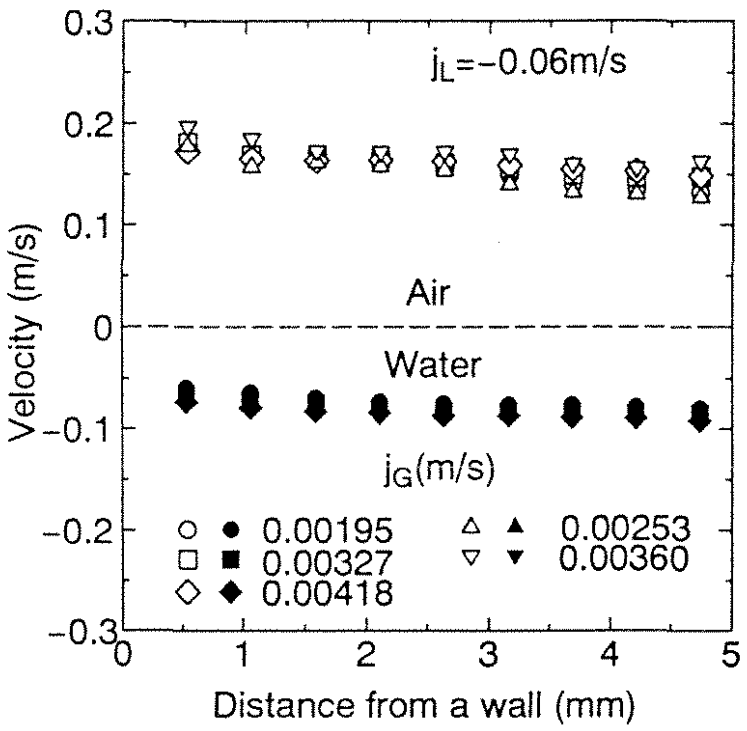

(a) Low water flow rate

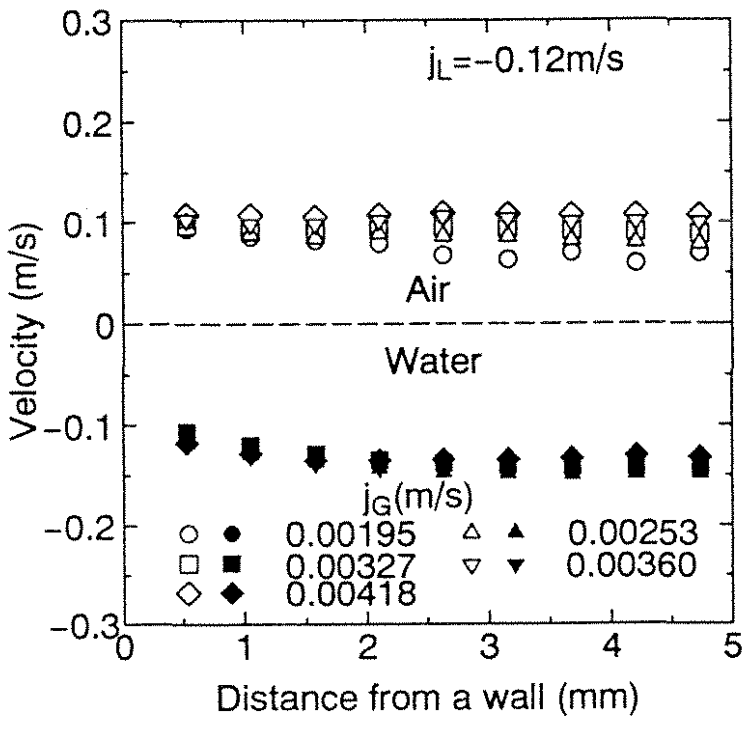

(b) High water flow rate

Fig.5 Velocity profiles of both phases in reference to air flow rates

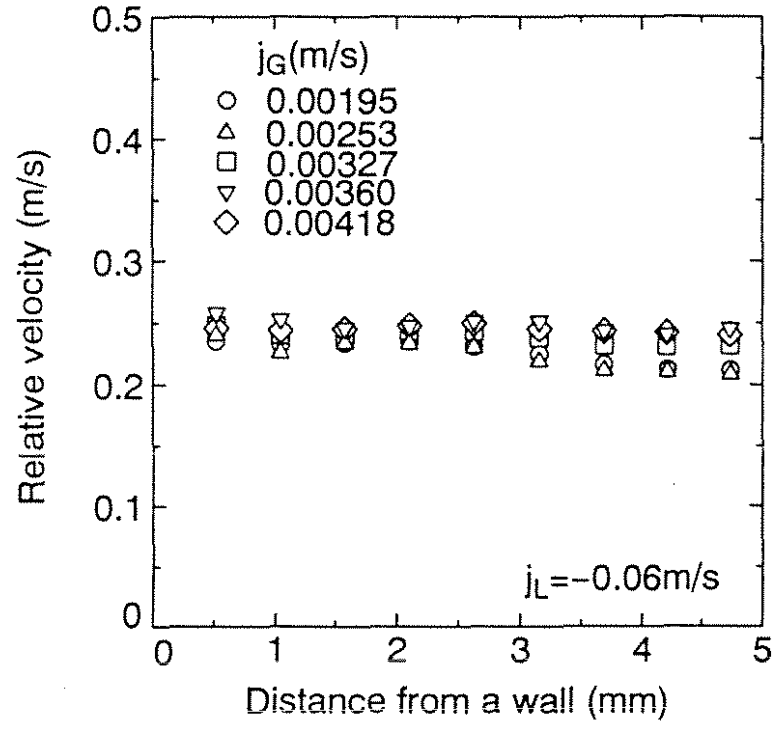

(a) Low water flow rate

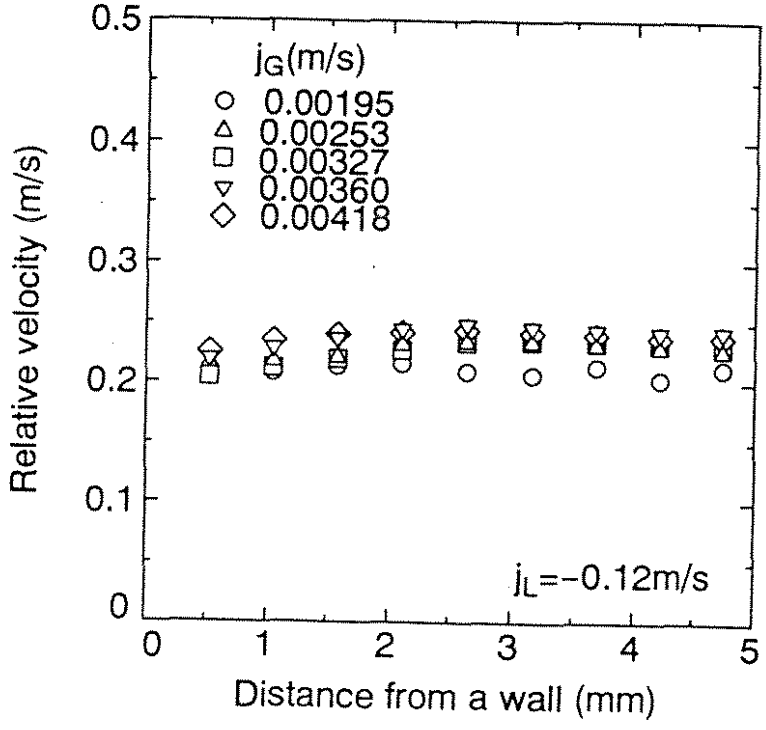

(b) High water flow rate

Fig.6 Relative velocity profiles in reference to air flow rates

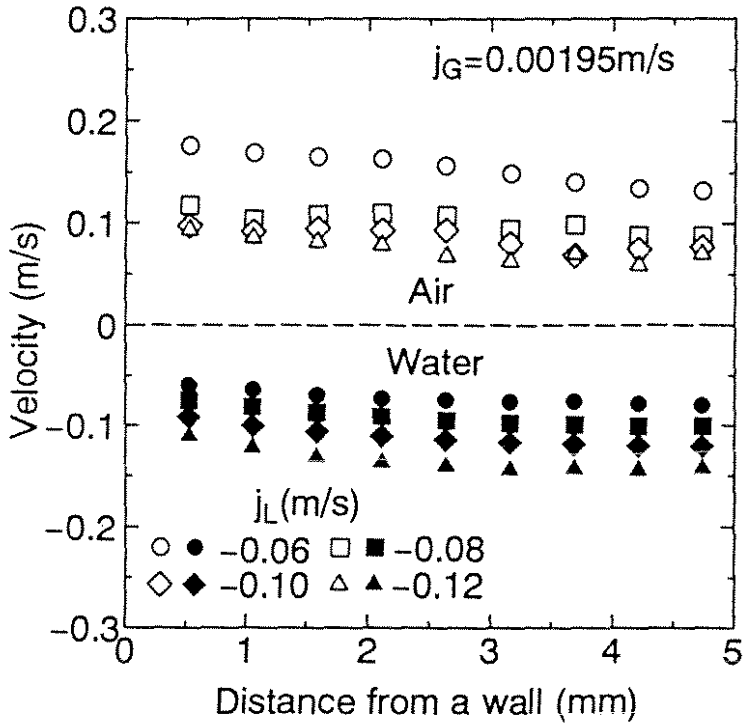

(a) Low air flow rate

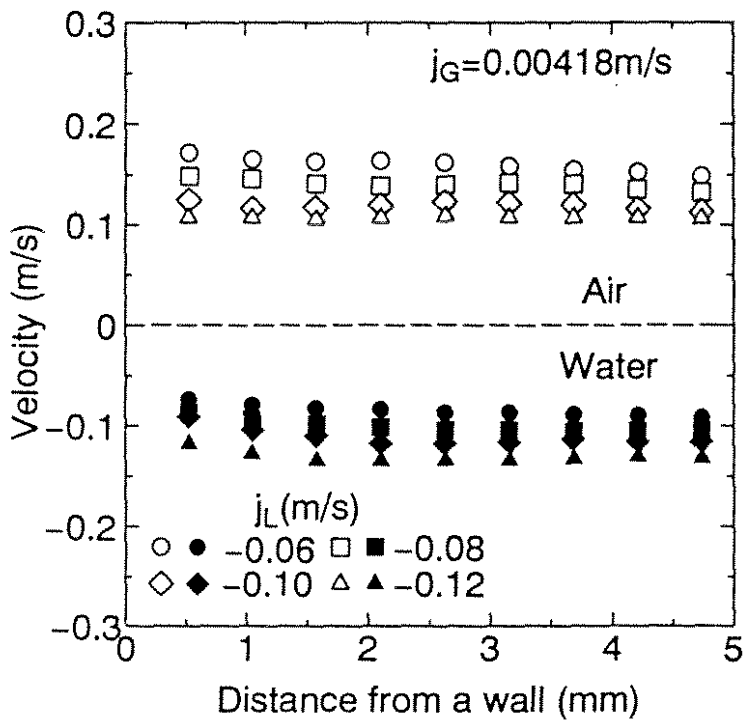

(b) High air flow rate

Fig.7 Velocity profiles of both phases in reference to water flow rates

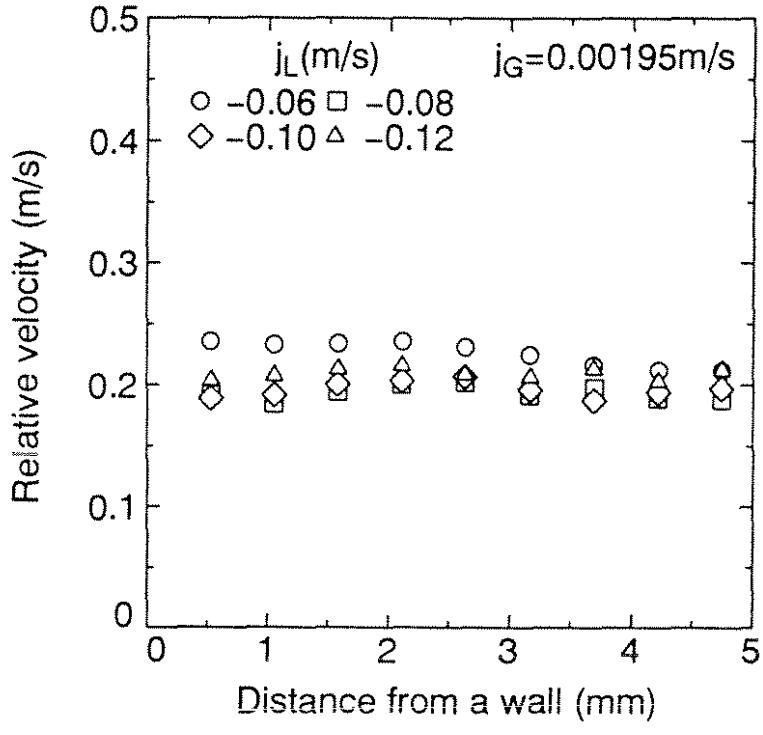

(a) Low air flow rate

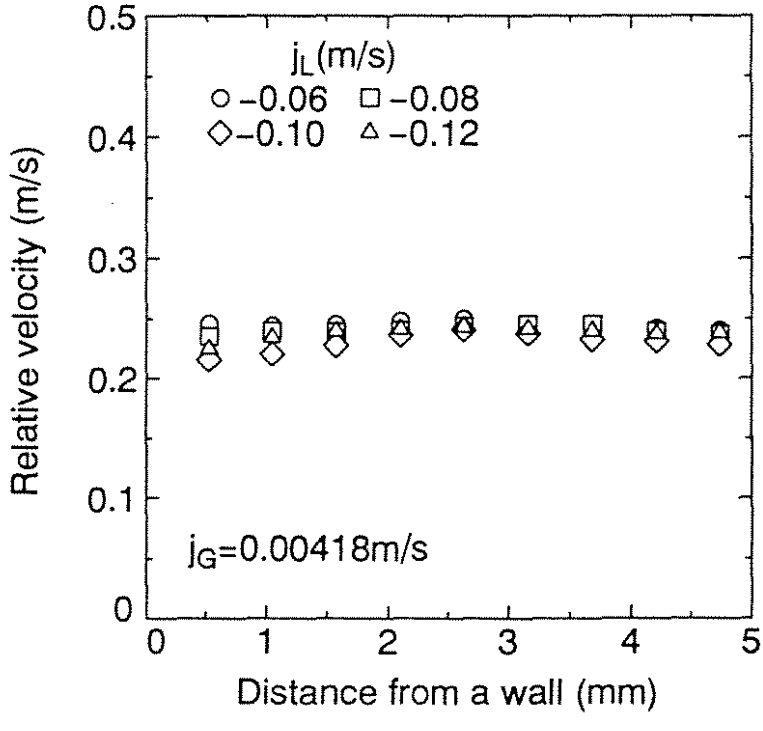

(b) High air flow rate

Fig.8 Relative velocity profiles in reference to water flow rates

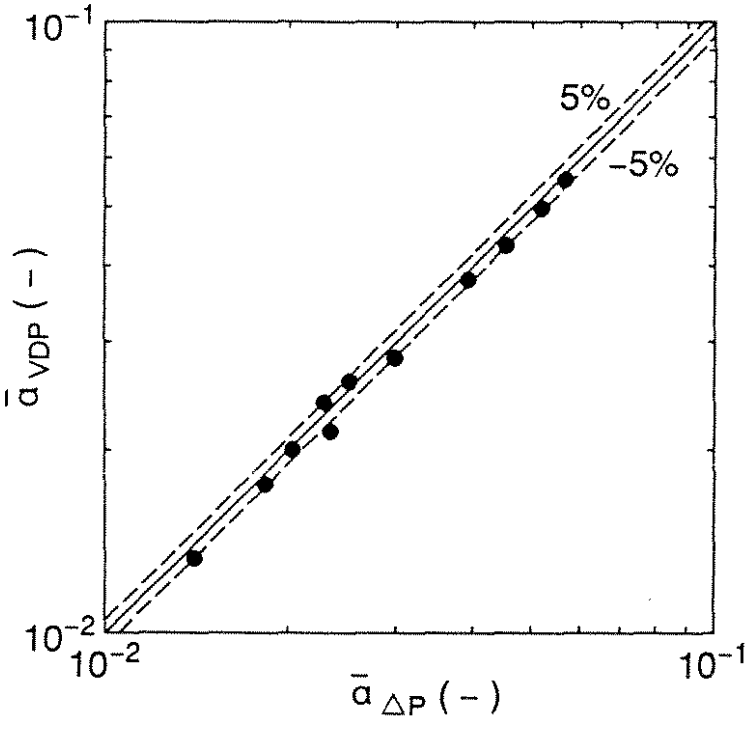

Fig.9 A comparison of average void fractions measured by hydrostatic head with those by the VDP

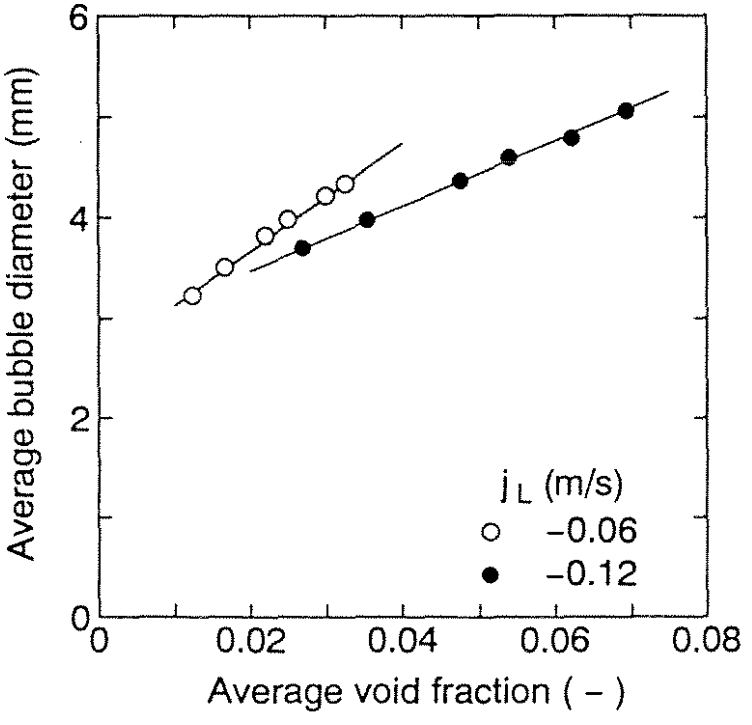

Fig.10 Average bubble diameter

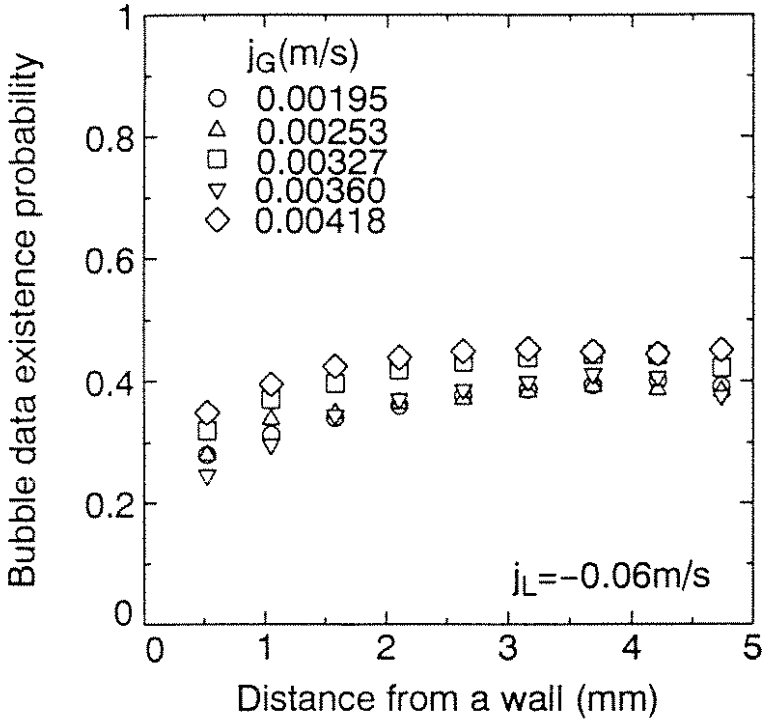

(a) Effect of air flow rates

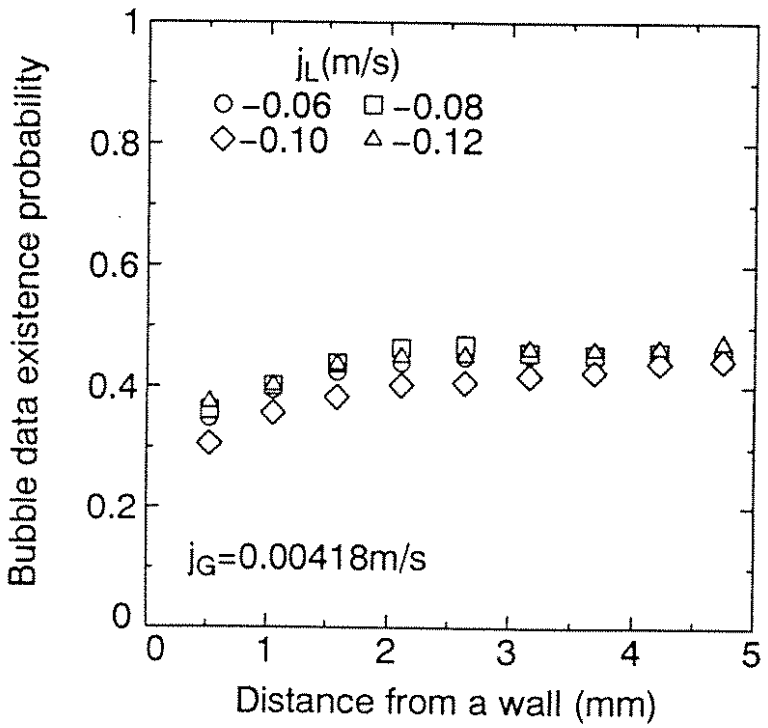

(b) Effect of water flow rates

Fig.11 Bubble data existence probability profiles in reference to air or water flow rates

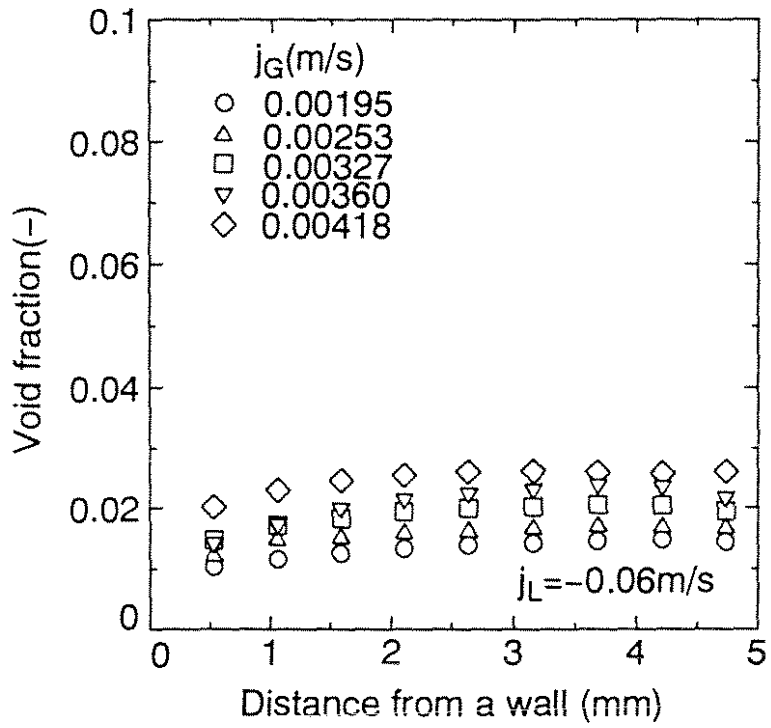

(a) Low water flow rate

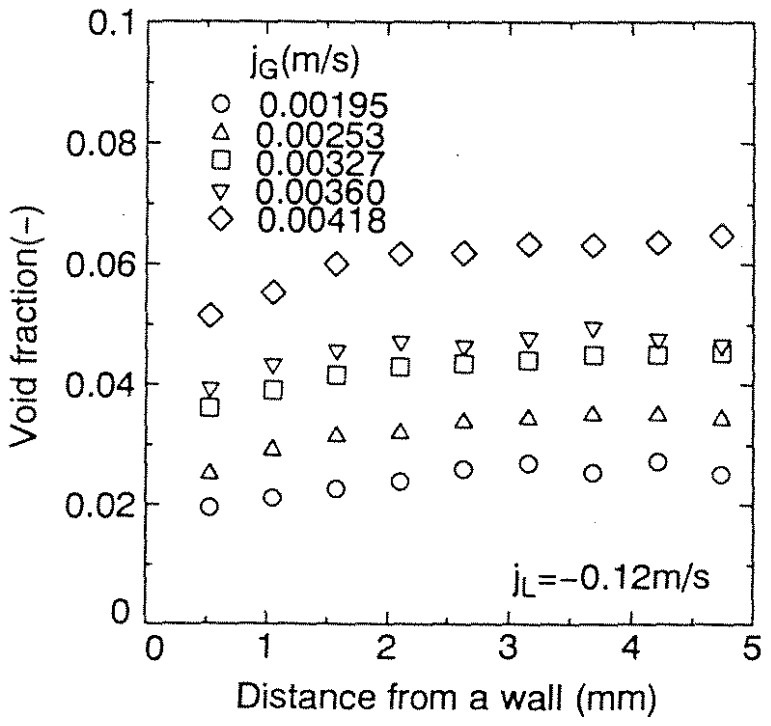

(b) High water flow rate

Fig.12 Void fraction profiles in reference to air flow rates

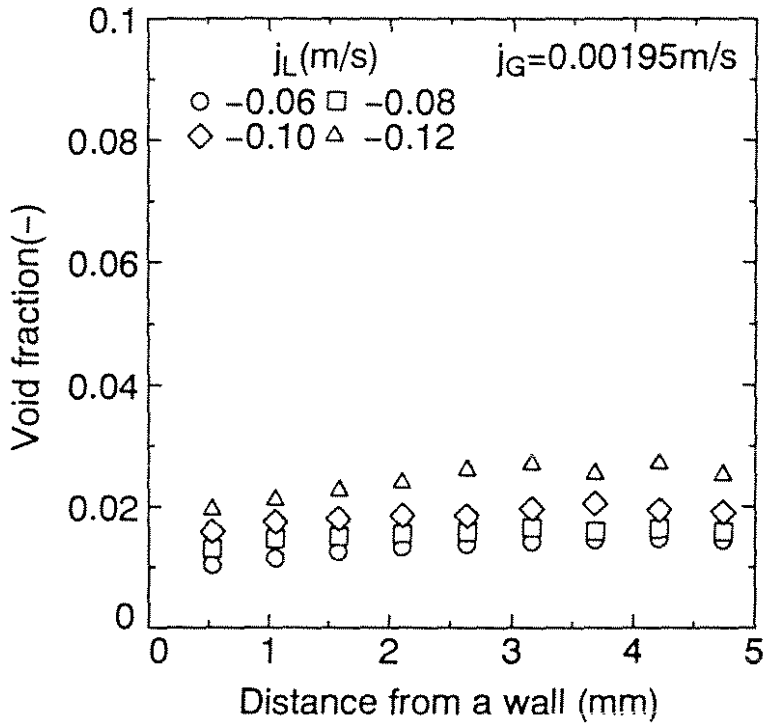

(a) Low air flow rate

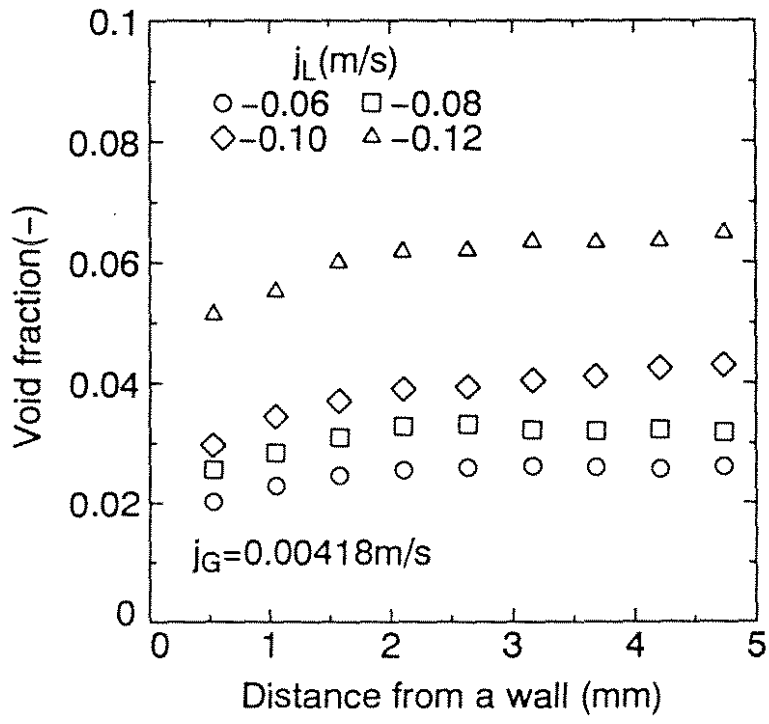

(b) Higher air flow rate

Fig.13 Void fraction profiles in reference to water flow rates

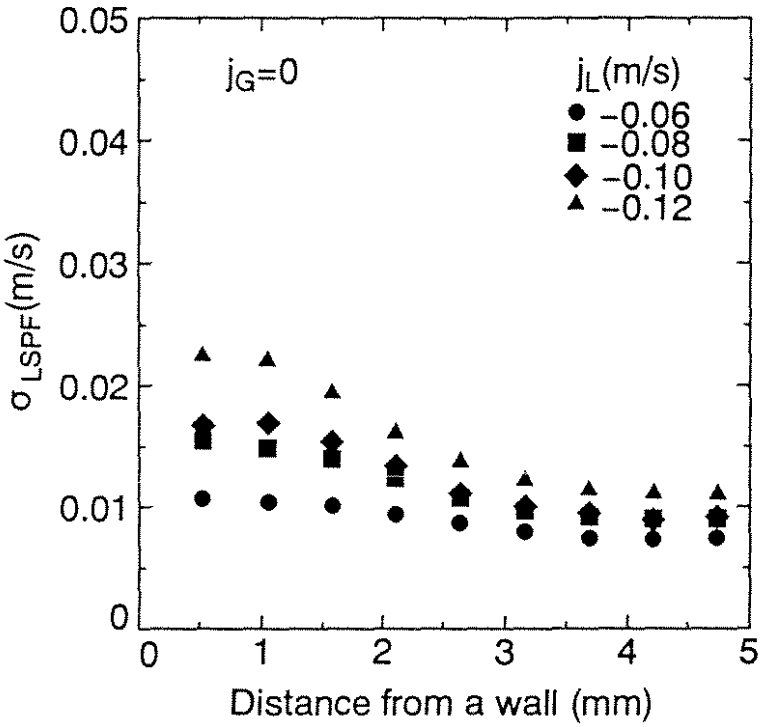

(a) Water downward flow

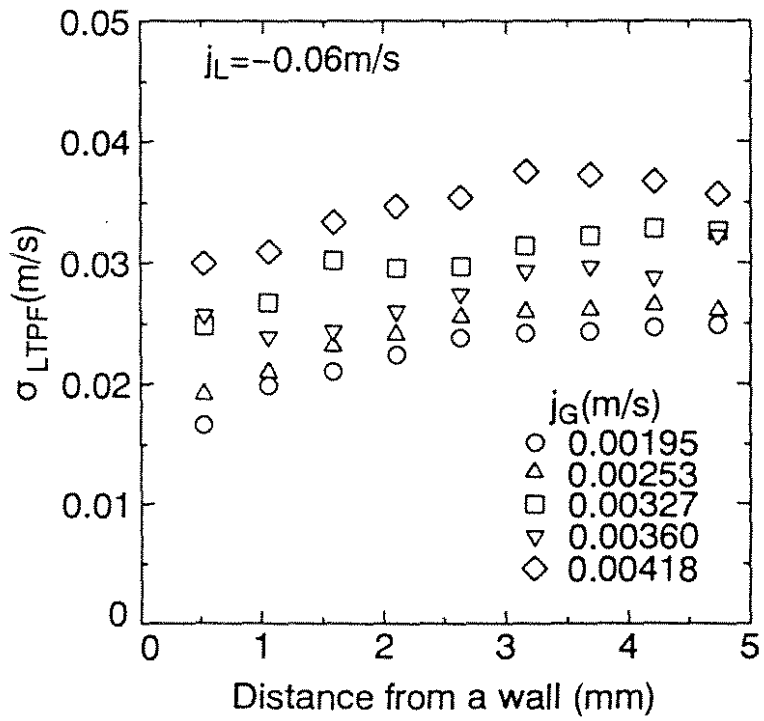

(b) Bubbly countercurrent flow

Fig.14 Typical standard deviation profiles of velocity fluctuation

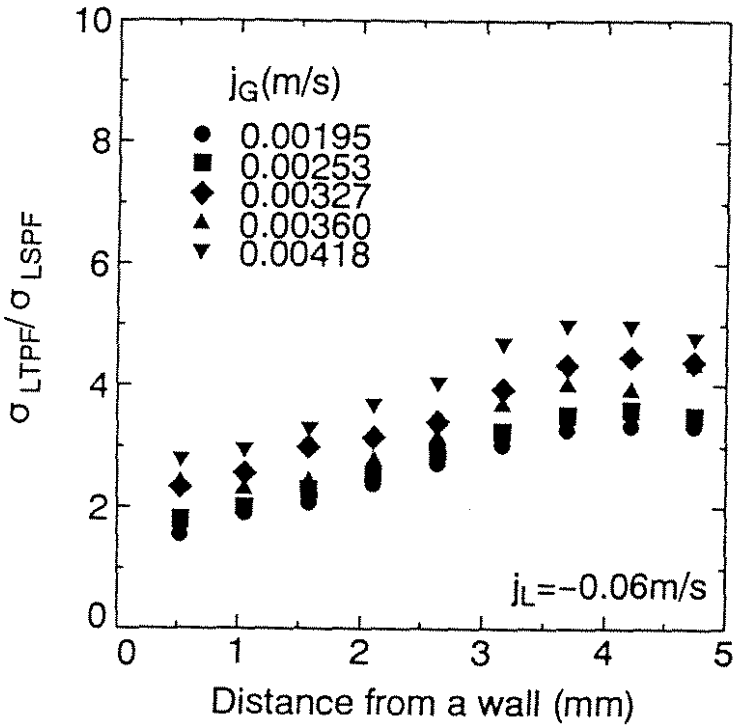

(a) Low water flow rate

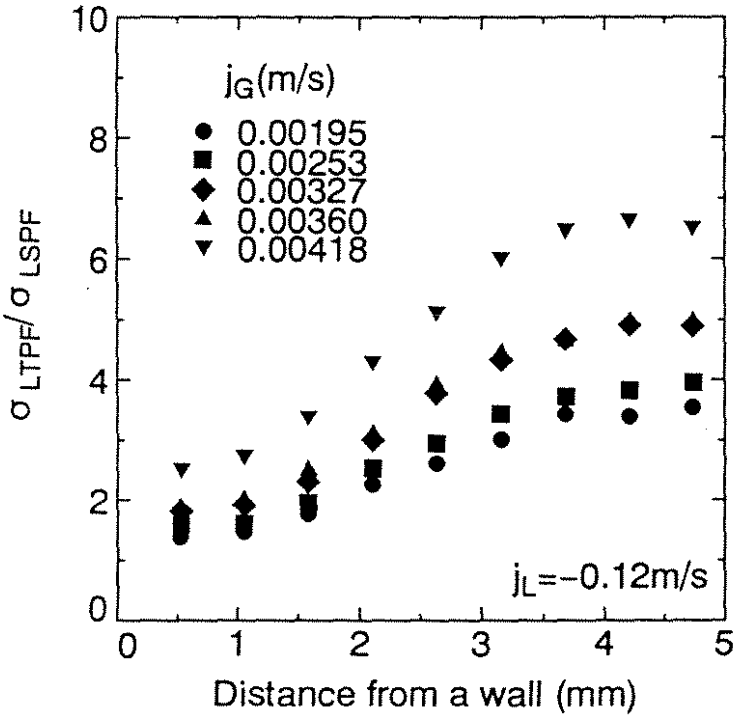

(b) High water flow rate

Fig.15 Turbulence intensity multiplier profiles

in bubbly countercurrent flows in reference to air flow rates

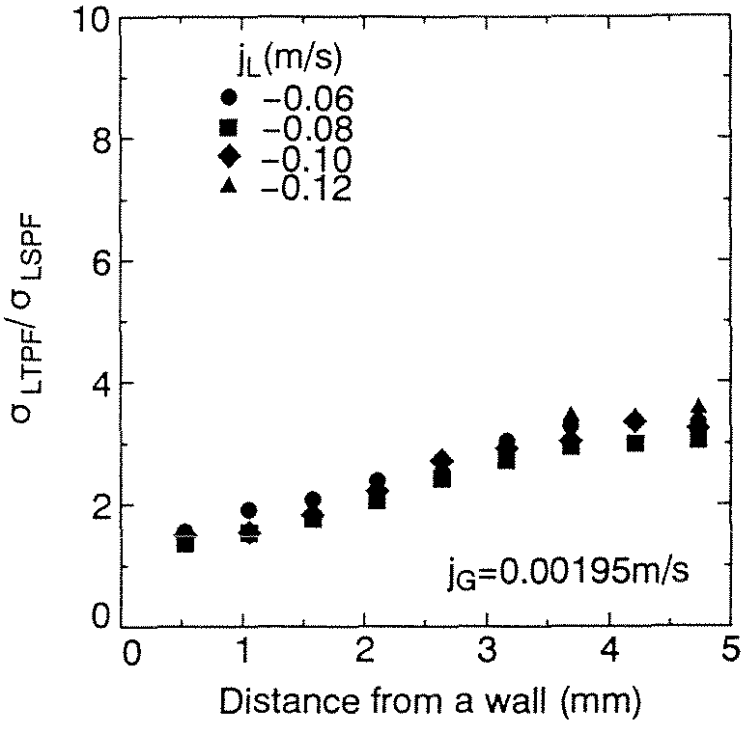

(a) Low air flow rate

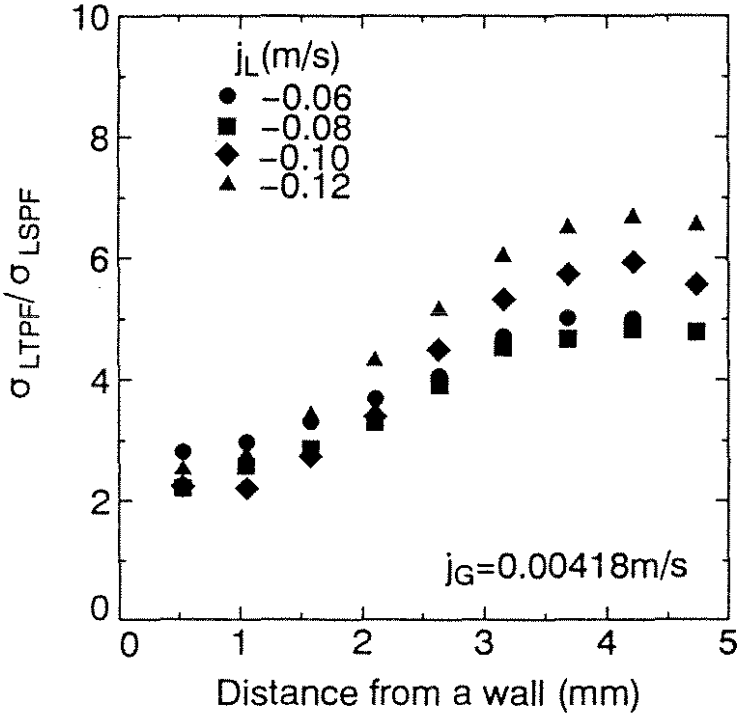

(b) High air flow rate

Fig.16 Turbulent intensity multiplier profiles

in bubbly countercurrent flows in reference to water flow rates

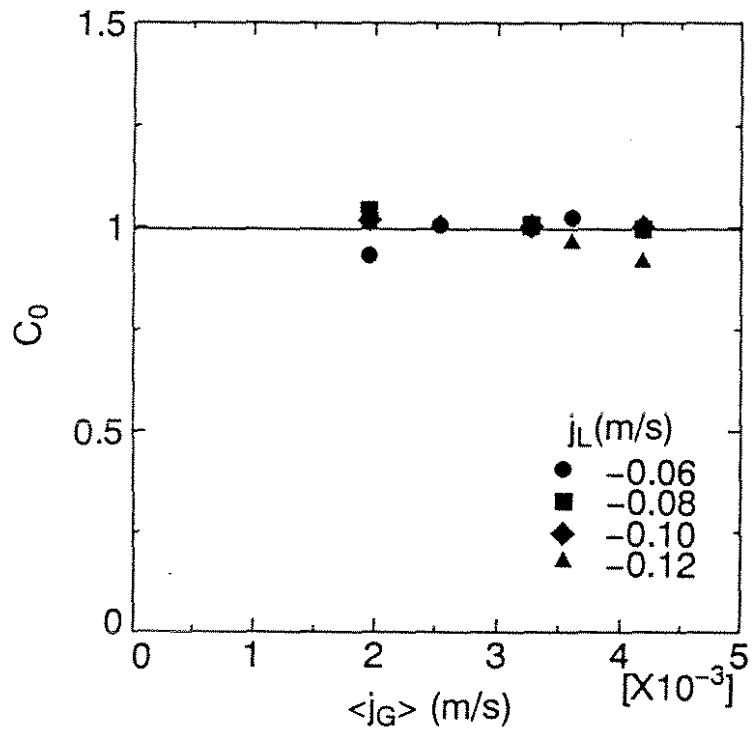

Fig.17 Distribution parameter of the drift flux model in bubbly countercurrent flow

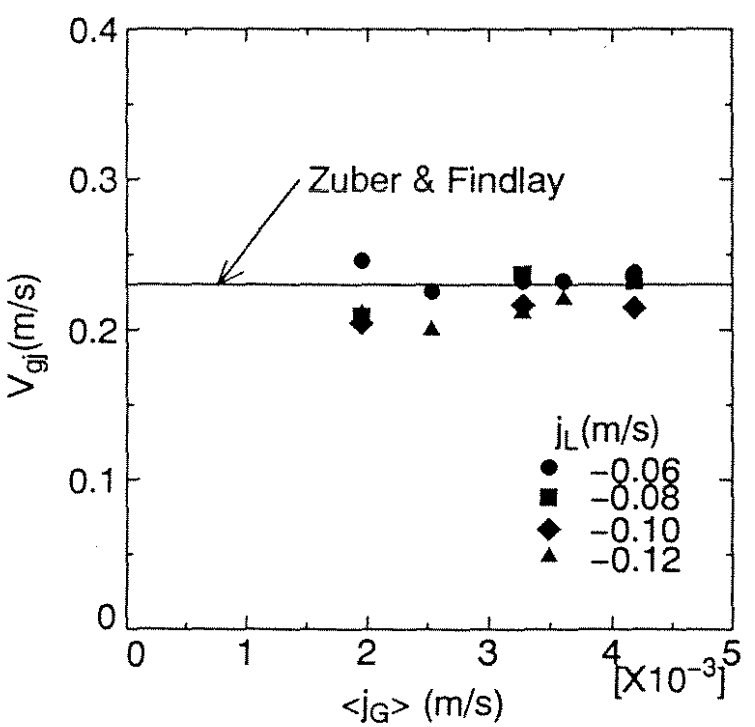

Fig.18 Drift velocity of the drift flux model in bubbly countercurrent flow